Supplementary Information

Mechanism of loading and translocation of type VI secretion system effector Tse6

Dennis Quentin, Shehryar Ahmad, Premy Shanthamoorthy, Joseph D Mougous, John C Whitney, Stefan Raunser

Supplementary Figures

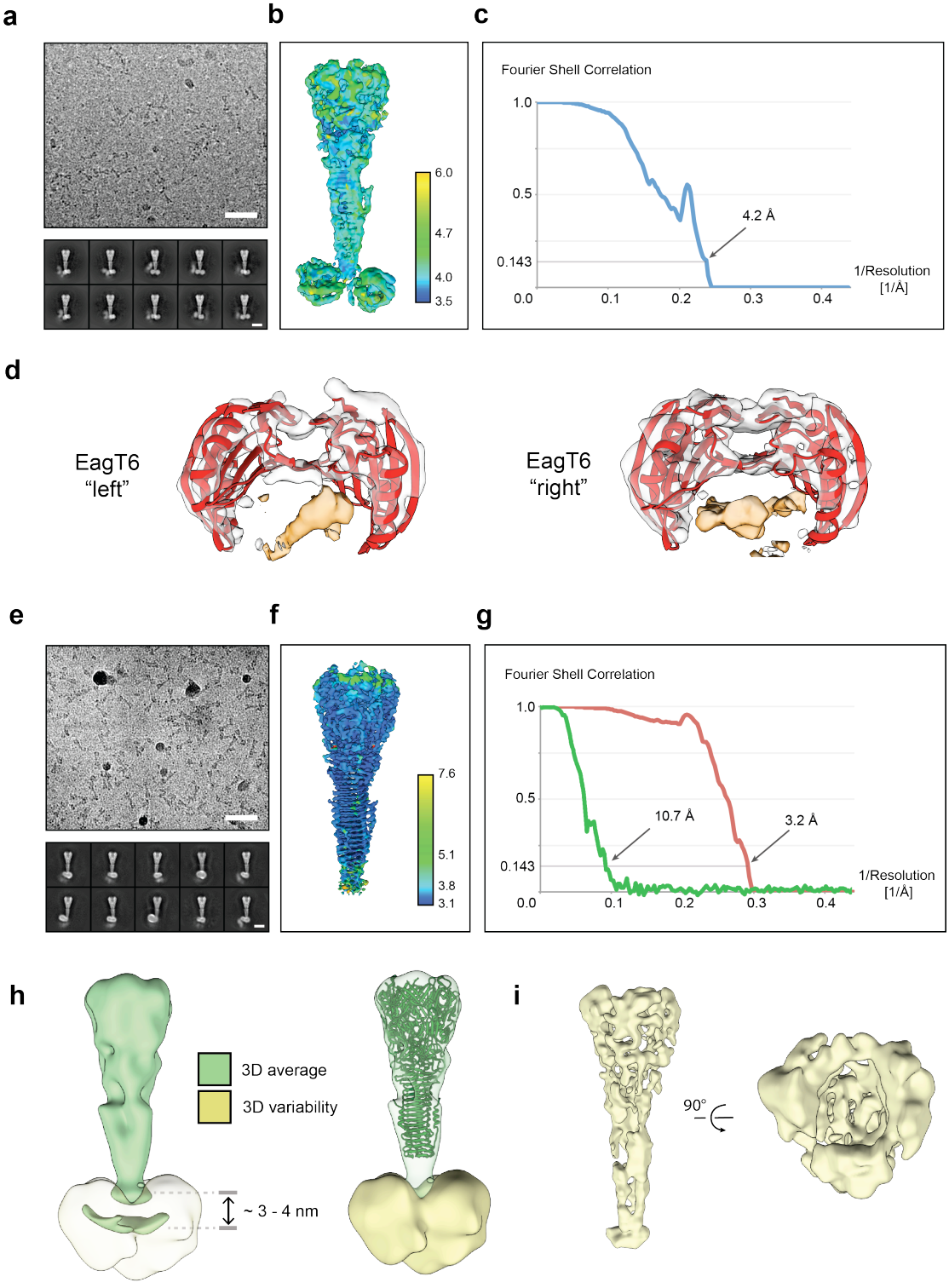

Supplementary Figure 1. Cryo-EM of the PFC and VgrG1-Tse6-EF-Tu complex in nanodiscs.

(**a**) Representative digital micrograph area of vitrified PFC (upper panel, scale bar: 50 nm) with corresponding representative class averages (lower panel, scale bar: 10 nm).

(**b**) Final 3D reconstruction of the PFC, comprising density for VgrG1, $Tse6_{PAAR}$, $Tse6_{TMDs}$, and $EagT6_2$, colored by local resolution. (**c**) FSC curve between two independently refined half-maps of the PFC (blue, 55,000 particles). (**d**) Top views of both EagT6 molecules shown with putative TMD density (orange) at different thresholds. EagT6 crystal structure (red) was fitted into EagT6 density (white). (**e**) Representative digital micrograph area of vitrified VgrG1-Tse6-EF-Tu complexes in nanodiscs (upper panel, scale bar: 50 nm) with corresponding representative class averages (lower panel, scale bar: 10 nm). (**f**) Final 3D reconstruction of the VgrG1-Tse6-EF-Tu complex in nanodiscs applying C3 symmetry colored by local resolution. Note that the other proteins of the complex are averaged out, because they do not have C3 symmetry. (**g**) FSC curves between two independently refined half-maps of the upper part of the Tse6-loaded VgrG1 complex in nanodiscs, applying C3 symmetry (red, 72,000 particles) and of a particle subset of the Tse6-loaded VgrG1 complex in nanodiscs in which the nanodisc was almost perpendicular to VgrG1, without applying symmetry (green, 11,000 particles). (**h**) Filtered 3-D average and 3-D variability densities indicate a high flexibility in the nanodisc region (lower part). (**i**) Side and top view of the 3-D reconstruction of the upper region of the VgrG1-Tse6-EF-Tu complex in nanodiscs, applying no symmetry. The strong influence of the nanodisc resulted in a distortion of the density corresponding to C3-symmetric VgrG1.

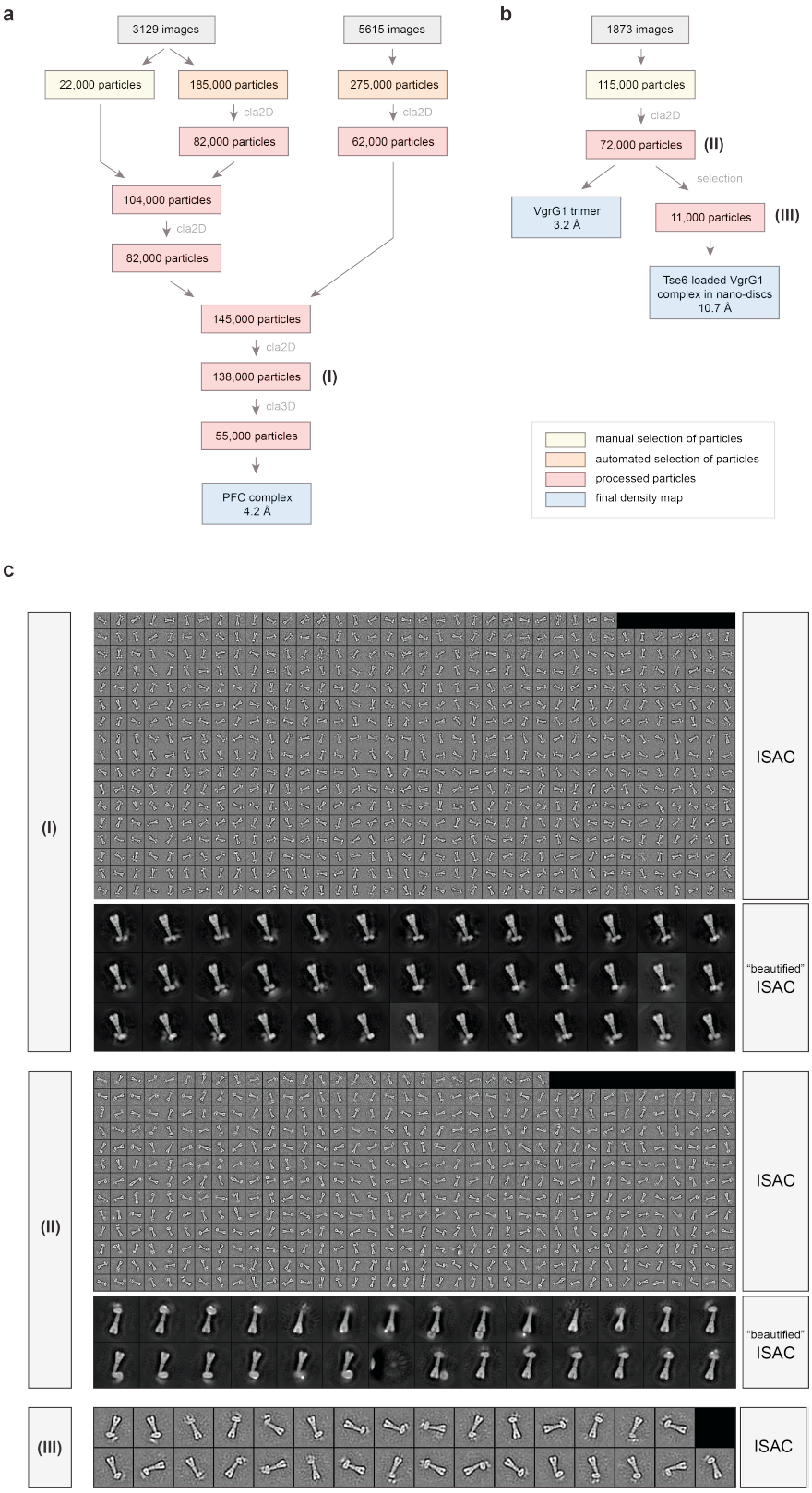

Supplementary Figure 2. Sorting trees of image processing in SPHIRE.

(**a**) Consecutive steps of 2-D- and 3-D-image processing for the PFC are shown as flowchart. The number of resulting particles is given after each step. (**b**) Same as in **a** for the Tse6-loaded VgrG1 complex in nanodiscs. While all 72,000 particles after 2-D

classification were used to resolve the upper region of the reconstituted complex, only a subset of 11,000 particles, in which the nanodisc was almost perpendicular to VgrG1, was used to obtain structural insights into its overall architecture. (**c**) 2-D class averages of the PFC (I) and Tse6-loaded VgrG1 complex in nanodiscs (II and III) corresponding to the final steps indicated in **a** and **b**. In addition to the binned 2-D class averages produced by ISAC that were used for the selection process, so called "beautified" class averages were calculated, showing unbinned data and thus high-resolution features.

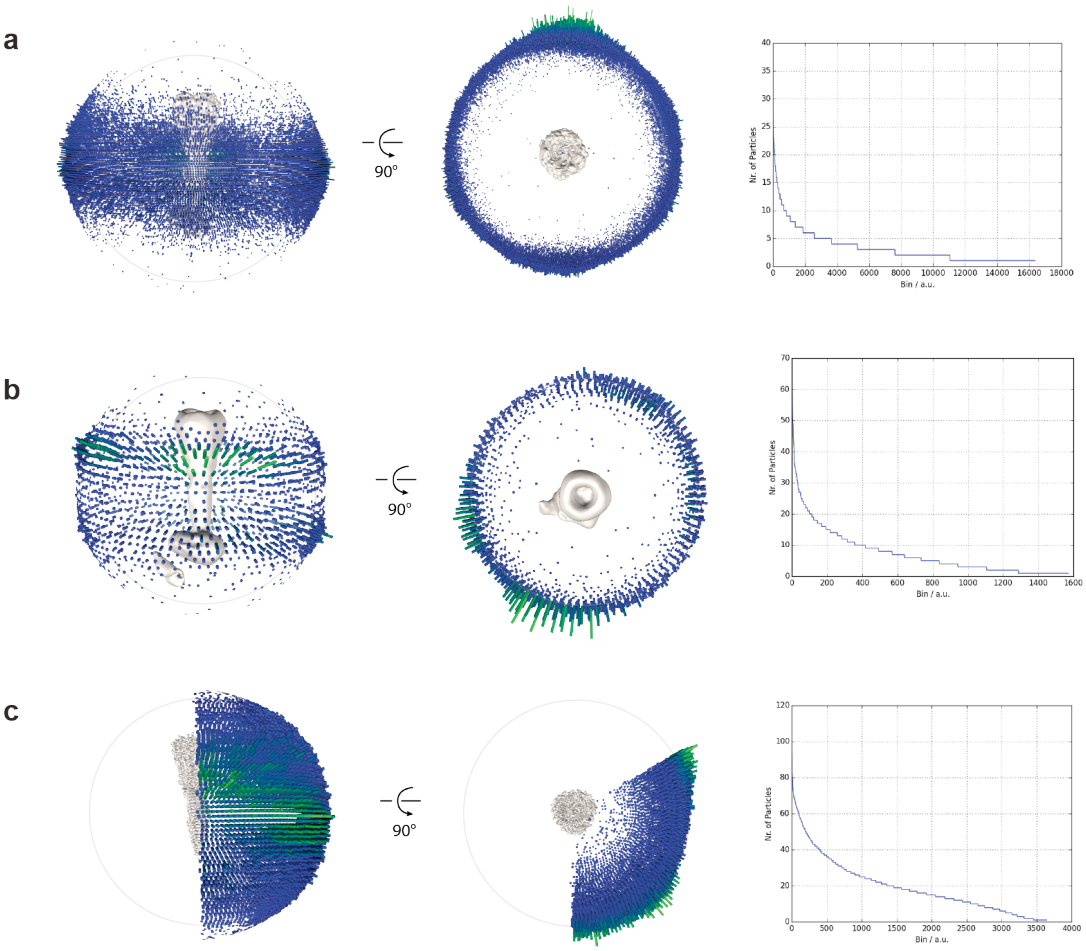

Supplementary Figure 3. 2-D- and 3-D-projection orientation plots.

(**a**) Side and top view of the 3-D angular distribution of PFC particles, in which the relative height of bars represents the number of particles. The corresponding 2-D histogram is shown on the right. (**b**) Same as in **a** for the reconstruction of the Tse6-loaded VgrG1 complex in nanodiscs, containing only particles in which the nanodisc is almost perpendicular to VgrG1. (**c**) Same as in **b**, except with all particles and C3 symmetry applied.

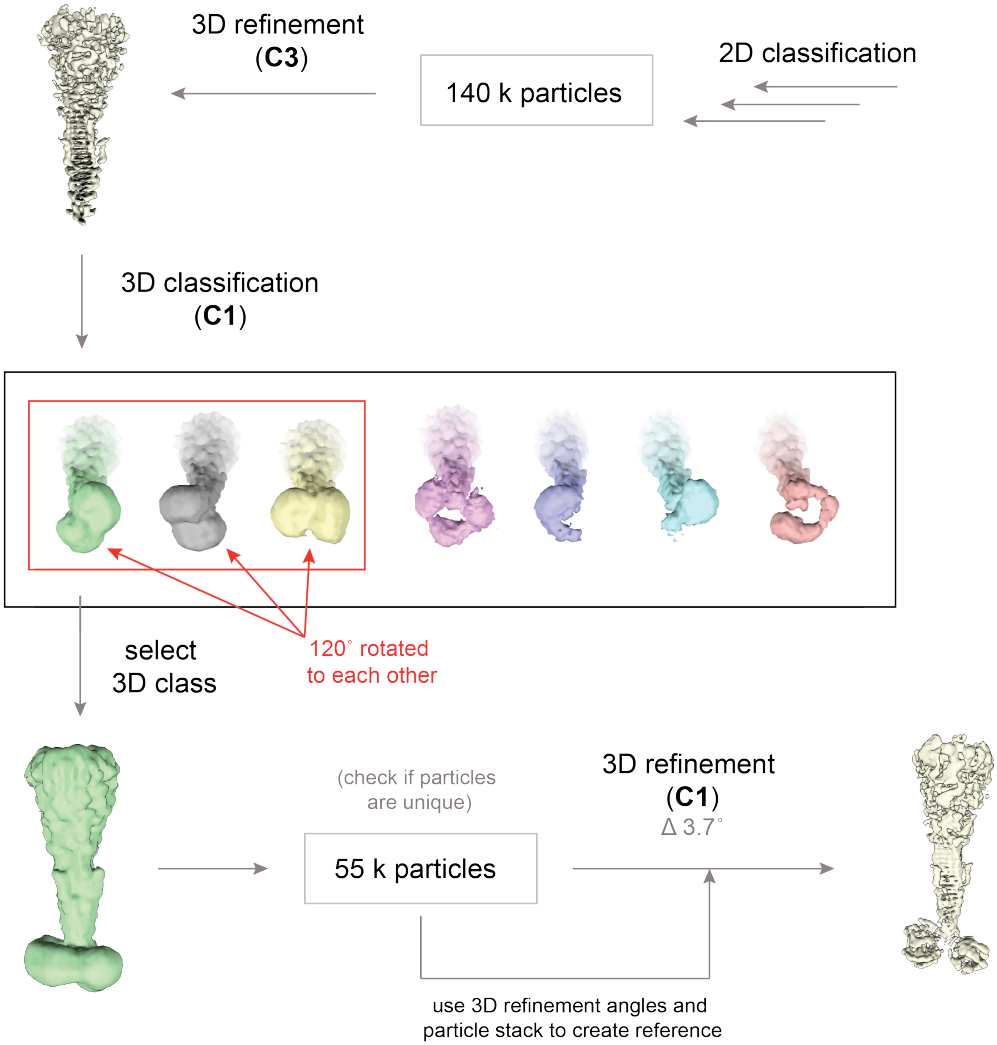

Supplementary Figure 4. Flowchart of image processing strategy in SPHIRE.

The 3-D refinement of the PFC was performed by imposing C3-symmetry. The determined three-dimensional projection parameters for each particle were subsequently used to create a symmetrized particle stack. This new stack contained three copies of each original particle with projection parameters rotated 120° along the (C3-) symmetry axis. The subsequent 3-D classification resulted in three volumes that were rotated by 120° to each other. As anticipated, the three copies of the original particle evenly distributed to these classes. However, given that classification procedures are not perfect in reality, we further confirmed that only one copy of the original particle is present in each class. Finally, one of the classes, containing 55,000 particles, was selected and subjected to a new local 3-D refinement without imposing symmetry. This resulted in the 4.2 Å density map of the PFC.

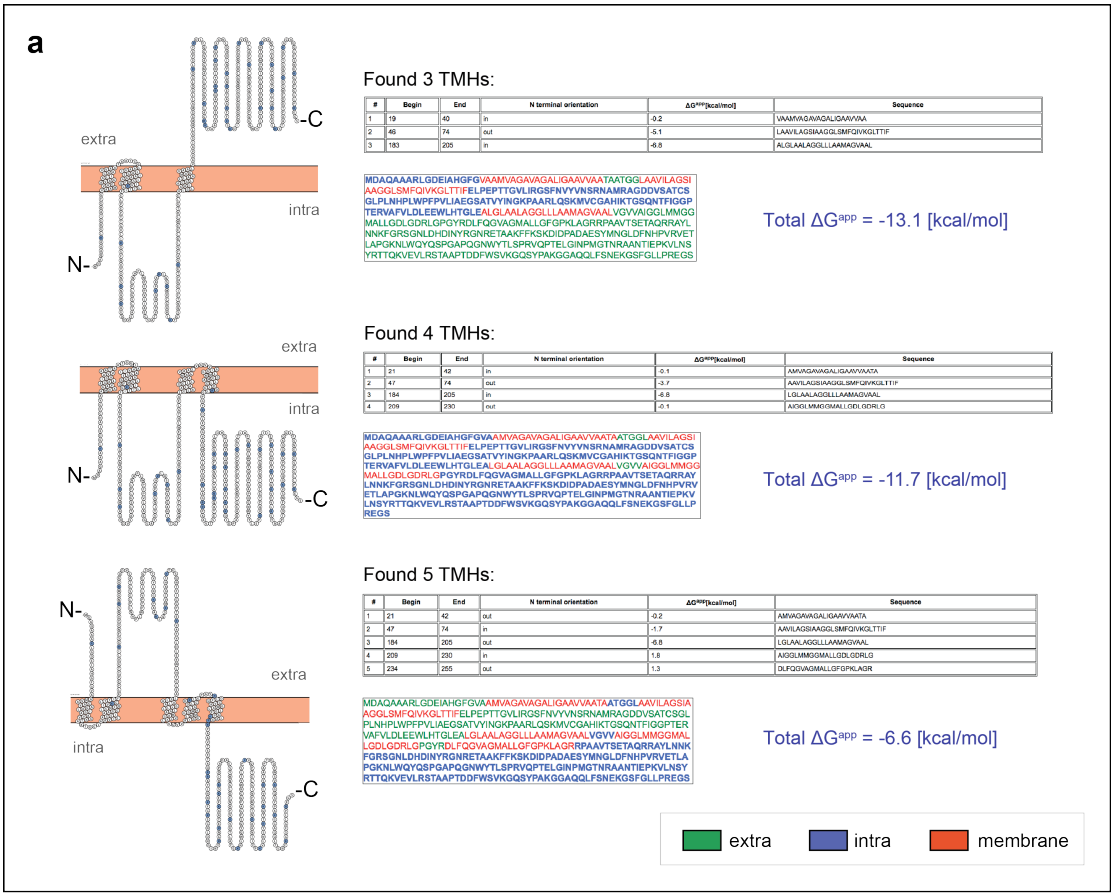

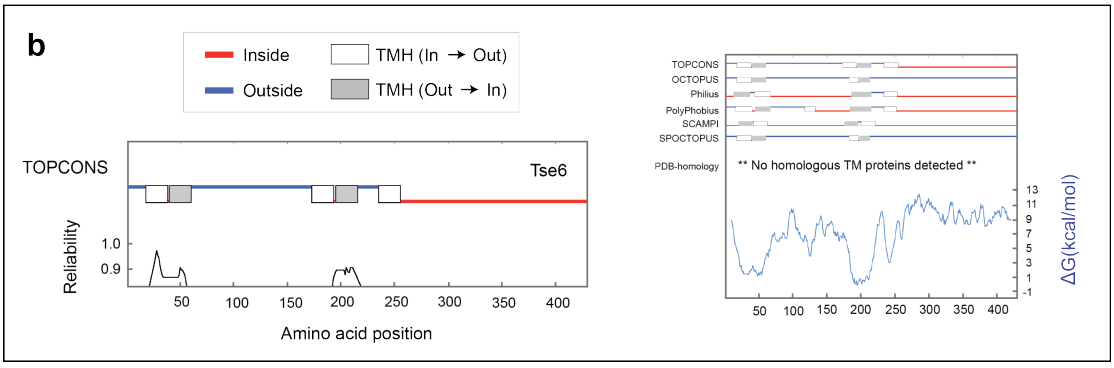

Supplementary Figure 5. Membrane topology prediction for Tse6.

(**a**) Three topology predictions of Tse6 featuring between three and five transmembrane helices (TMHs). The predictions have been obtained by the TopGraph server, which is based on membrane insertion profiles, calculated using sdTβL. (**b**) TOPCONS consensus predictions of Tse6, combining results of the most common topology prediction servers to generate a consensus prediction of Tse6 topology featuring 5 transmembrane helices.

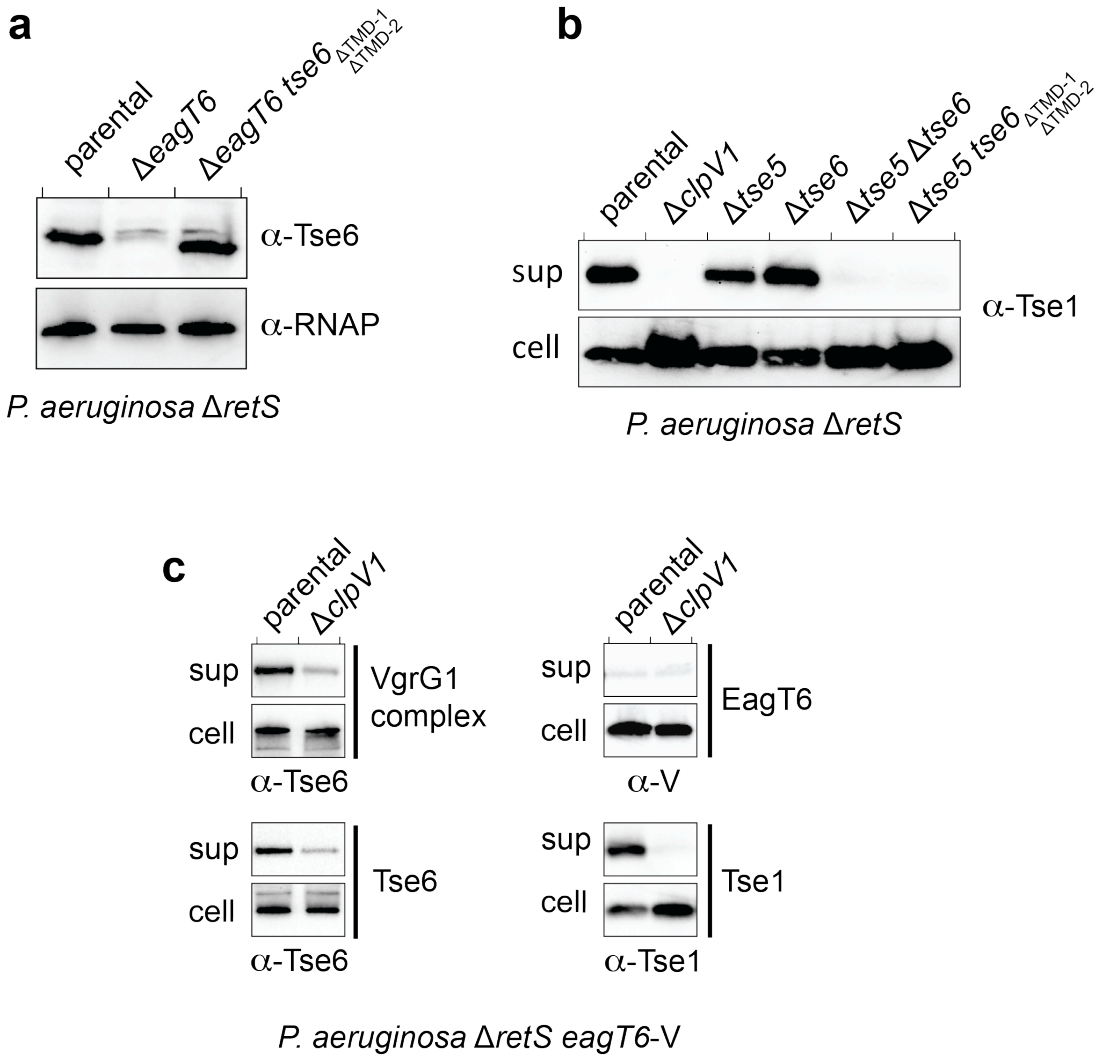

Supplementary Figure 6. Secretion and growth experiments in *P. aeruginosa*.

(**a**) Western blot analysis of Tse6 levels in the indicated *P. aeruginosa* strains shows that EagT6 is no longer required for *in vivo* Tse6 stability when both TMDs are deleted. The T6S ATPase ClpV1 provides the energy necessary to drive the secretion apparatus. A strain lacking the ClpV1-encoding gene *clpV1* thus mimics inactivated (H1-) T6SS. (**b**) Secretion assays of T6S effector Tse1 in *P. aeruginosa.* In the absence of the only two PAAR-containing proteins, Tse5 and Tse6, the T6S apparatus cannot function anymore (no secretion of Tse1). Deletion of both TMDs of Tse6 in a strain lacking *tse5* has the same effect. (**c**) Secretion assay in the indicated *P. aeruginosa* strains shows that, in contrast to VgrG1, Tse6 and Tse1, EagT6 is not secreted from the cell and is required for the stability of Tse6 but not $Tse6_{\Delta TMD1\ \Delta TMD2}$.

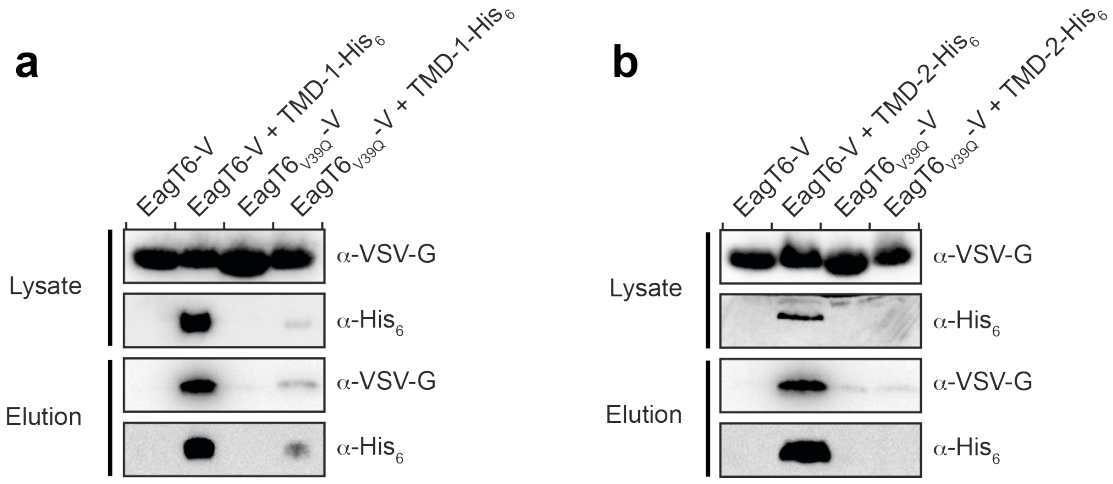

Supplementary Figure 7. Interaction of EagT6 with the TMDs of Tse6.

(**a**) Pull downs of the TMD-1 of Tse6 with EagT6. Western blot analysis of VSV-G and His_6 levels indicate binding of TMD-1 to EagT6. Mutation of valine 39, that is located within the hydrophobic cavity of EagT6, to glutamine abolishes TMD-1 binding. (**b**) Same as in **a** for TMD-2. Similar as for TMD-1, EagT6 pulls down with TMD-2 and the V39Q mutation abolishes binding.

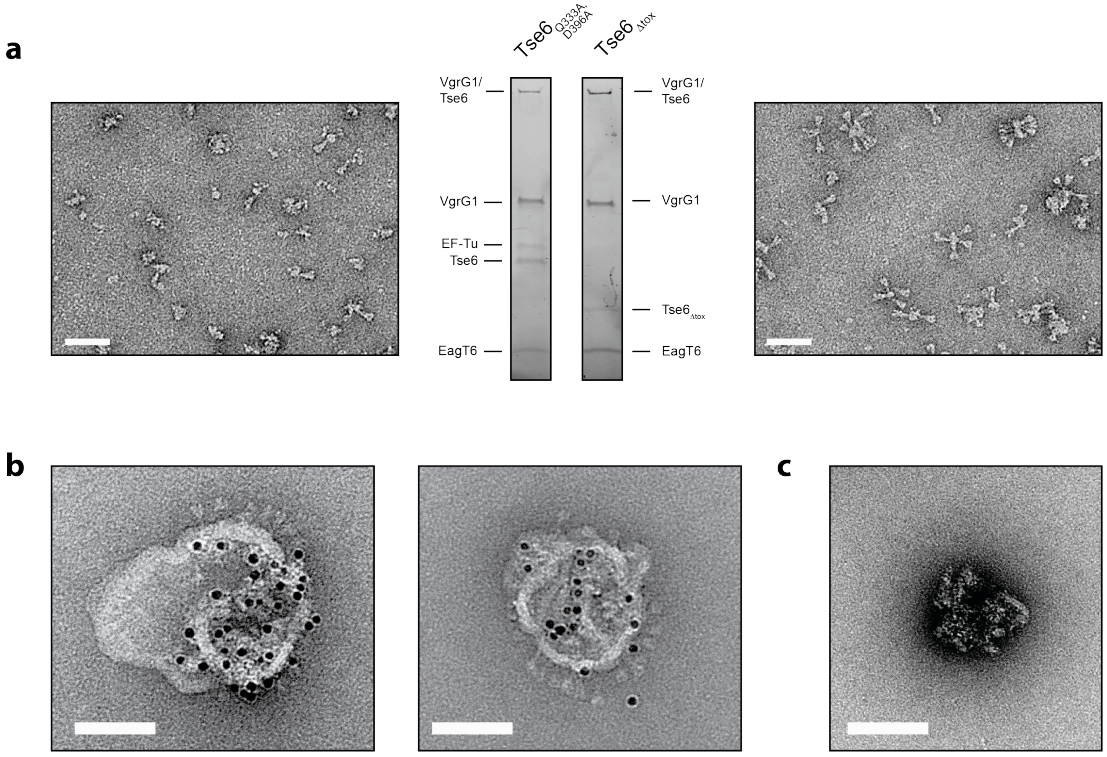

Supplementary Figure 8. Catalytically inactive and toxin-domain lacking mutants of Tse6.

(**a**) Representative negatively stained electron micrograph areas of complexes containing a catalytically inactive Tse6 double mutant ($Tse6_{Q333A,\ D396A}$) (left panel) and a Tse6 mutant lacking its C-terminal toxin domain ($Tse6_{\Delta tox}$) (right panel). Corresponding SDS-PAGE is shown in the middle. Scale bars: 50 nm. (**b**) Electron micrograph area showing Tse6-loaded VgrG1 complex reconstituted in liposomes and labeled with 5 nm NTA-coated nanogold. Scale bar: 50 nm. (**c**) Electron micrograph area showing liposome fraction after incubation with $Tse6_{\Delta tox}$ -loaded VgrG1 complex. Complexes lacking $Tse6_{tox}$ do not readily insert into the lipid bilayer of liposomes. Scale bar: 100 nm.

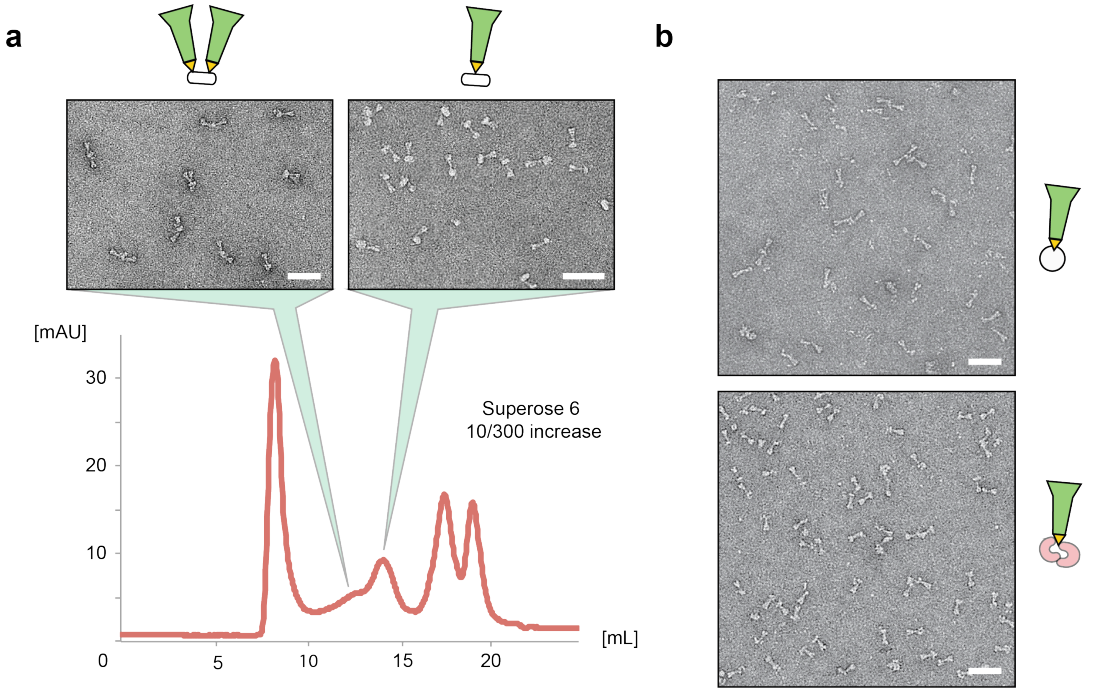

Supplementary Figure 9. Purification of the Tse6-loaded VgrG1 complex after reconstitution into nanodiscs.

(**a**) Size exclusion chromatography of Tse6-loaded VgrG1 reconstituted into preformed nanodiscs (MSP1D1-ΔH5). Representative areas of negatively stained micrographs of fractions containing the complex in nanodiscs are shown. Scale bars: 50 nm. (**b**) Representative micrographs of Tse6-loaded VgrG1 complex in detergent (upper panel) and PFC (lower panel). Scale bars: 50 nm.

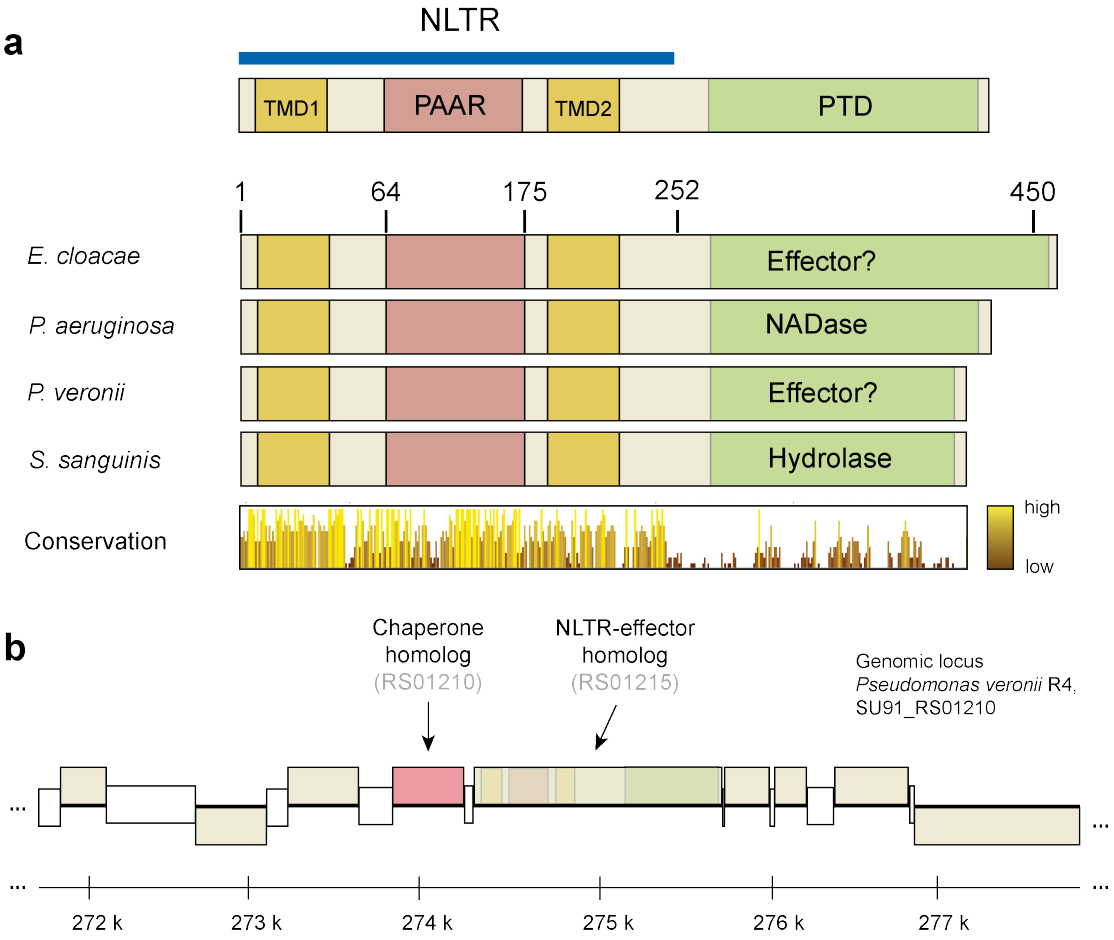

Supplementary Figure 10. Conserved domain architecture of the N-terminal loading and translocation region of T6S effectors.

(**a**) Comparison of the domain organization (top) and multiple sequence alignment (bottom) of T6S effectors of selected members of the *Proteobacteria* phylum shows conservation of the N-terminal loading and translocation region (NLTR, blue) and high variability of the C-terminal polymorphic toxin domain (PTD, green). The core of the NLTR is formed by the transmembrane domains (TMD1, TMD2, yellow) and the PAAR domain (dark red). (**b**) Genomic context in *P. veronii R4* of a homologue of Tse6 and its respective chaperone, homologous to EagT6. The gene coding for the chaperone is located upstream of NLTR-effector gene. The colors of NLTR-effector gene, indicating domains are the same as in **a**.

Supplementary Figure 11. Multiple sequence alignment highlights conservation of NTLR domain.

(**a**) Graphical representation (WebLogo) based on a multiple sequence alignment of selected members of α-,β- and γ- *proteobacteria*. Predicted domain boundaries are illustrated with colored boxes above the logos. TMDs are shown in orange, the PAAR domains in red and the PTD in green. (**b**) Multiple sequence alignment (Clustal Omega) of nine selected Gram-negative bacteria with corresponding phylogenetic tree, highlighting the conservation of the NTLR. Color code as in **a**.

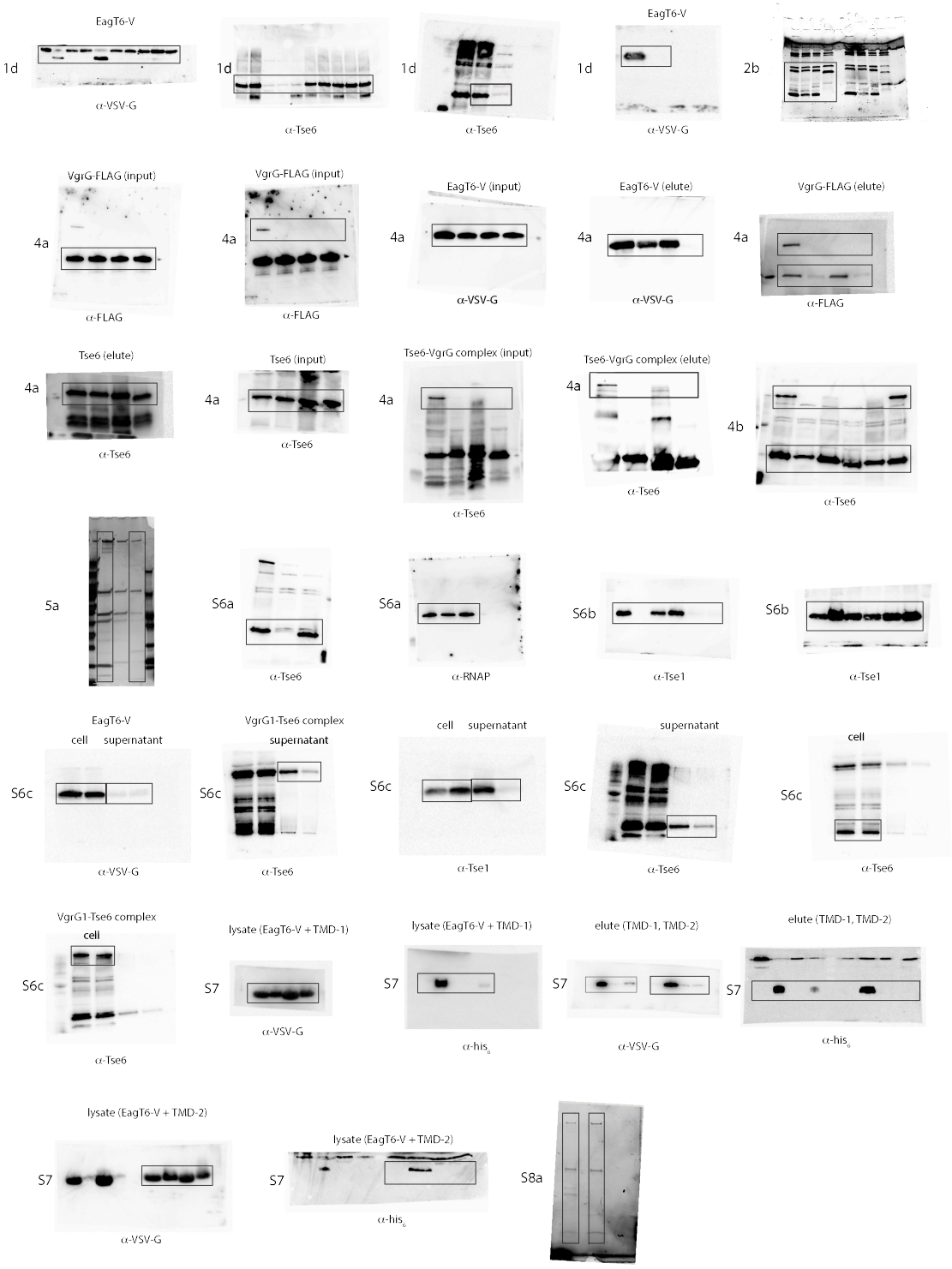

Supplementary Figure 12. Full-length raw versions of gels and blots.

Unmanipulated full-length versions of all gel- and blot- images with corresponding figure numbers. Sections that are shown are highlighted with black boxes.

Supplementary Tables

Supplementary Table 1. Model refinement of VgrG1 in the PFC and VgrG1-Tse6-EF-Tu complex in nanodiscs.

	PFC			VgrG1-Tse6-EF-Tu complex in ND				
	4MTK (incl. B-factor)	C1-Refinement **C1**-Rosetta	C1-Refinement **C1**-Rosetta (incl. B-factor)	**4MTK** (incl. B-factor)	C3-Refinement **C1**-Rosetta	C3-Refinement **C1**-Rosetta (incl. B-factor)	C3-Refinement **C3**-Rosetta	C3-Refinement **C3**-Rosetta (incl. B-factor)
Wt	25	25	25	25	25	25	25	25
Ramachandran Outliers	0.05	0.91	0.91	0.05	0.7	0.7	2.09	2.09
Ramachandran Favored	96.09	91.44	91.44	96.09	94.65	94.65	91.17	91.17
Rotamer Outliers	5.45	0.06	0.06	5.45	0.0	0.0	0.95	0.95
C-beta Deviation	0.0	0.0	0.0	0.0	0.0	0.0	0.0	0.0
Clashscore	10.06	4.50	4.50	9.82	1.26	1.26	1.71	1.71
RMS Bonds	0.0038	0.0152	0.0152	0.0037	0.0145	0.0145	0.0143	0.0143
RMS Angles	1.17	1.53	1.53	1.17	1.35	1.35	1.26	1.26
Mol Probity Score	2.35	1.73	1.73	2.34	1.22	1.22	1.44	1.44
EM Ringer Score	0.533135	0.461668	0.461668	2.951283	4.548322	4.548322	4.283487	4.283487
FSC Work	0.205372	0.311012	0.31492	0.578509	0.594187	0.606926	0.594811	0.602522
FSC Free	0.191802	0.286383	0.29067	0.5771	0.576787	0.582562	0.572111	0.575408

Supplementary Table 2. Strains used in this study.

Organism	Genotype	Description	Reference
P. aeruginosa PAO1	wild-type		Stover et al., 2000
	ΔPA4856	*retS* deletion parent strain	Goodman et al., 2004
	ΔPA4856 attB::*lacZ*	Constitutive *lacZ* expression strain, Tet^R	Whitney et al., 2014
	ΔPA4856 ΔPA0092 ΔPA0093 attB::*lacZ*	*tse6 tsi6* deletion strain constitutively expressing *lacZ*, Tet^R	Whitney et al., 2014
	ΔPA4856 ΔPA0090	*clpV1* deletion strain	Hood et al., 2010
	ΔPA4856 ΔPA0094	*eagT6* deletion strain	Whitney et al., 2015
	ΔPA4856 ΔPA4427	*sspB* deletion strain	Silverman et al., 2013
	ΔPA4427 ΔPA4856 *tsi6*-D4	*sspB* deletion strain expressing Tsi6 with a C-terminal DAS+4 tag	Whitney et al., 2015
	ΔPA4856 ΔPA4427 PA0093_ΔTMD-1_ ΔTMD-2	*sspB* deletion strain expressing Tse6 variant lacking residues 2-61 and 180-222	This study
	ΔPA4427 ΔPA4856 *tsi6*-D4 PA0093_ΔTMD-1_ ΔTMD-2	*sspB* deletion strain expressing Tsi6 with a C-terminal DAS+4 tag and a Tse6 variant lacking residues 2-61 and 180-222	This study
	ΔPA4856 PA0094-V	Expresses EagT6 fused to a C-terminal VSV-G epitope tag	Whitney et al., 2015
	ΔPA4856 ΔPA0090 PA0094-V	*clpV1* deletion strain expressing EagT6 with a C-terminal VSV-G tag	Whitney et al., 2015
	ΔPA4856 PA0094-V_L3Q	Expresses EagT6_L3Q variant	This study
	ΔPA4856 PA0094-V_Q20A	Expresses EagT6_Q20A variant	This study
	ΔPA4856 PA0094-V_I22Q	Expresses EagT6_I22Q variant	This study
	ΔPA4856 PA0094-V_R34A	Expresses EagT6_R34A variant	This study
	ΔPA4856 PA0094-V_V39Q	Expresses EagT6_V39Q variant	This study
	ΔPA4856 PA0094-V_D48A	Expresses EagT6_D48A variant	This study
	ΔPA4856 PA0094-V_K64A	Expresses EagT6_K64A variant	This study
	ΔPA4856 PA0094-V_T115Q	Expresses EagT6_T115Q variant	This study
	ΔPA4856 PA0094-V_H125A	Expresses EagT6_H125A variant	This study
	ΔPA4856 PA0094-V_R140A	Expresses EagT6_R140A variant	This study
	ΔPA4856 PA0093_ΔTMD-1	Expresses Tse6 variant lacking residues 2-61	This study
	ΔPA4856 PA0093_ΔTMD-2	Expresses Tse6 variant lacking residues 180-222	This study
	ΔPA4856 PA0093_ΔTMD-1_ ΔTMD-2	Expresses Tse6 variant lacking residues 2-61 and 180-222	This study
	ΔPA4856 ΔPA0091	*vgrG1* deletion strain	Whitney et al., 2014
	ΔPA4856 ΔPA2685	*vgrG4* deletion strain	This study
	ΔPA4856 ΔPA0094 PA0093_ΔTMD-1_ ΔTMD-2	*eagT6* deletion strain expressing Tse6 variant lacking residues 2-61 and 180-222	This study
	ΔPA4856 ΔPA2684	*tse5* deletion strain	This study
	ΔPA4856 ΔPA0093	*tse6* deletion strain	Whitney et al., 2014
	ΔPA4856 ΔPA2684 ΔPA0093	*tse5 tse6* deletion strain	This study
	ΔPA4856 ΔPA2684 PA0093_ΔTMD-1_ ΔTMD-2	*tse5* deletion strain expressing Tse6 variant lacking residues 2-61 and 180-222	This study
E. coli SM10 λpir	Km^R, *thi-1 thr leu tonA lac Y supE recA*::RP4-2-Tc::Mu, pir	Conjugation strain	BioMedal LifeScience
E. coli XL-1 Blue	*recA1 endA1 gyrA96 thi-1 hsdR17 supE44 relA1 lac* [F′ *proAB* $lacI^q$ ZΔ*M15* Tn*10* (Tet^R)]	Cloning strain	Agilent
E. coli BL21 (DE3) CodonPlus	F^- ompT gal dcm lon $hsdS_B(r_B^- m_B^-)$ λ(DE3) pLysS(cm^R)	Protein expression strain	Novagen

Supplementary Table 3. Plasmids used in this study.

Plasmid	Relevant features	Reference
pEXG2	Allelic replacement vector containing *sacB*, Gm^R	Rietsch et al., 2005
pPSV35-CV	Expression vector with *lacI*, *lacUV5* promoter, C-terminal VSV-G tag, Gm^R	Mougous et al., 2006
pPSV38-CV	Expression vector with *lacI*, *lacUV5* promoter, C-terminal VSV-G tag, Gm^R	Castang et al., 2008
pSCrhaB2-CV	Expression vector with *PrhaB*, Tmp^R	Cardona and Valvano, 2005
pETDuet-1	Co-expression vector with *lacI*, T7 promoter, N-terminal His_6 tag in MCS-1, Amp^R	Novagen
pRSFDuet-1	Co-expression vector with *lacI*, T7 promoter, N-terminal His_6 tag in MCS-1, Kan^R	Novagen
pEXG2::PA0092_DAS+4	For generating strains encoding Tsi6 with a C-terminal DAS+4 tag (DENYSENYADAS)	Whitney et al., 2015
pEXG2::PA0093_ΔTMD-1	For generating strains encoding Tse6 lacking residues 2-61	This study
pEXG2::PA0093_ΔTMD-2	For generating strains encoding Tse6 lacking residues 180-222	This study
pEXG2::PA0093_ΔTMD-1_ΔTMD-2	For generating strains encoding Tse6 lacking residues 2-61 and 180-222	This study
pEXG2::ΔPA0094*	Alternate *eagT6* deletion allele in pEXG2. 3' flank lacks region of *tse6* encoding residues 2-61	This study
pEXG2::PA0094_L3Q	For generating strains encoding EagT6 L3Q point mutant	This study
pEXG2::PA0094_Q20A	For generating strains encoding EagT6 Q20A point mutant	This study
pEXG2::PA0094_I22Q	For generating strains encoding EagT6 I22Q point mutant	This study
pEXG2::PA0094_R34A	For generating strains encoding EagT6 R34A point mutant	This study
pEXG2::PA0094_V39A	For generating strains encoding EagT6 V39A point mutant	This study
pEXG2::PA0094_D48A	For generating strains encoding EagT6 D48A point mutant	This study
pEXG2::PA0094_K64A	For generating strains encoding EagT6 K64A point mutant	This study
pEXG2::PA0094_T115Q	For generating strains encoding EagT6 T115Q point mutant	This study
pEXG2::PA0094_H125A	For generating strains encoding EagT6 H125A point mutant	This study
pEXG2::PA0094_R140A	For generating strains encoding EagT6 R140A point mutant	This study
pEXG2::ΔPA2684	*tse5* deletion allele in pEXG2	This study
pEXG2::ΔPA2685	*vgrG4* deletion allele in pEXG2	Whitney et al., 2014
pEXG2:: ΔPA4427	*sspB* deletion allele in pEXG2	Silverman et al., 2013
pPSV35-CV::PA0094	Expression vector for *eagT6*	Whitney et al., 2015
pPSV38-CV::PA4427	Expression vector for *sspB*	Castang and Dove, 2012
pSCrhaB2-CV::PA0093_D396A	Expression vector for $tse6_{D396A}$	This study
pSCrhaB2-CV::PA0093_D396A_ΔTMD-1_ΔTMD-2	Expression vector for $tse6_{D396A, \Delta 2\text{-}61, \Delta 180\text{-}222}$	This study
pSCrhaB2-CV::$PA0093_{tox}$_D396A	Expression vector for $tse6_{282\text{-}430, D396A}$	This study
pETDuet-1::PA0091_FLAG	Expression vector for C-terminally FLAG-tagged *vgrG1*	This study
pETDuet-1::PA0093 ::PA0092	Co-expression vector for *tse6* and *tsi6*	Whitney et al., 2015
pETDuet-1::PA0093_ΔTMD-1 ::PA0092	Co-expression vector for $tse6_{\Delta 2\text{-}61}$ and *tsi6*	This study
pETDuet-1::PA0093_ΔTMD-2 ::PA0092	Co-expression vector for $tse6_{\Delta 180\text{-}222}$ and *tsi6*	This study
pETDuet-1::PA0093_ΔTMD-1_ΔTMD-2 ::PA0092	Co-expression vector for $tse6_{\Delta 2\text{-}61, \Delta 180\text{-}222}$ and *tsi6*	This study
pRSFDuet-1::PA0091 ::PA0094	Expression vector for *vgrG1* and *eagT6*	Whitney et al., 2015
pETDuet-1:: PA0093_Q333A_D396A ::PA0092	Co-expression vector for $tse6_{Q333A, D396A}$ and *tsi6*	This study
pETDuet-1::PA0093Δtox ::PA0092	Co-expression vector for $tse6_{1\text{-}281}$ and *tsi6*	This study
pETDuet-1::PA0093_TMD-1 ::PA0094-V	Co-expression vector for $tse6_{2\text{-}61}$ and *eagT6*	This study
pETDuet-1::PA0093_TMD-2 ::PA0094-V	Co-expression vector for $tse6_{180\text{-}222}$ and *eagT6*	This study
pETDuet-1::PA0093_TMD-1 ::PA0094-V_V39Q	Co-expression vector for $tse6_{2\text{-}61}$ and $eagT6_{V39Q}$	This study
pETDuet-1::PA0093_TMD-2::PA0094-V_V39Q	Co-expression vector for $tse6_{180\text{-}222}$ and $eagT6_{V39Q}$	This study
pETDuet-1::PA0094-V	Expression vector for *eagT6*	This study
pETDuet-1::PA0094-V_V39Q	Expression vector for $eagT6_{V39Q}$	This study